Electronic Supplementary Material

Activated carbon-hybridized and amine-modified polyacrylonitrile nanofibers toward ultrahigh and recyclable metal ion and dye adsorption from wastewater

Fengli Li[1], Chuang Chen[1], Yuda Wang[1], Wenpeng Li[1], Guoli Zhou (✉)[1], Haoqin Zhang[1], Jie Zhang (✉)[1], Jingtao Wang[1, 2]

1 School of Chemical Engineering, Zhengzhou University, Zhengzhou 450001, China

2 Henan Institute of Advanced Technology, Zhengzhou University, Zhengzhou 450003, China

E-mails: zglcumt@126.com (Zhou G); zhanglianbi@zzu.edu.cn (Zhang J)

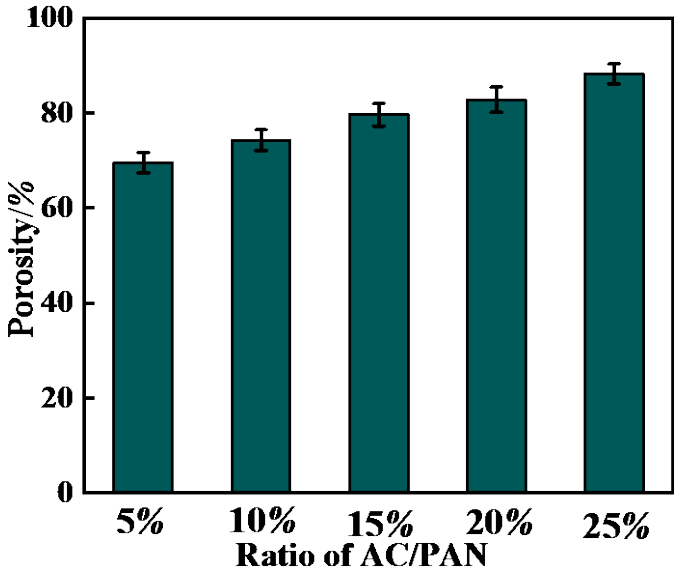

Fig. S1 The porosity of PAN/AC nanofibers with containing different ratios of AC.

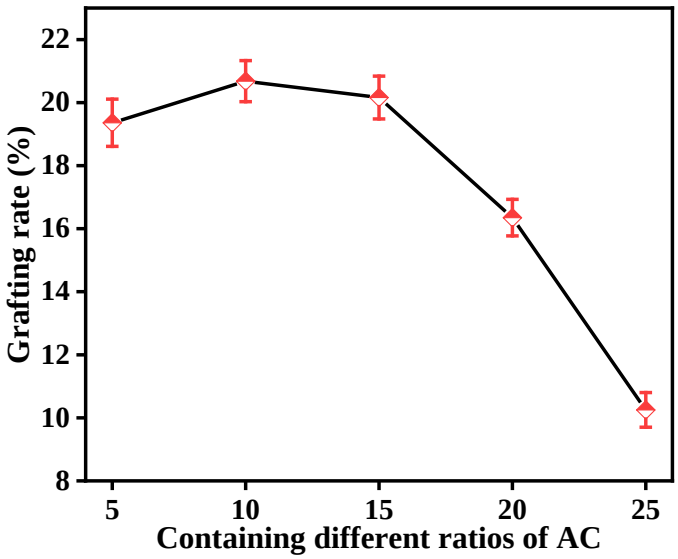

Fig. S2 The grafting rate of PAN/AC nanofibers with containing different ratios of AC.

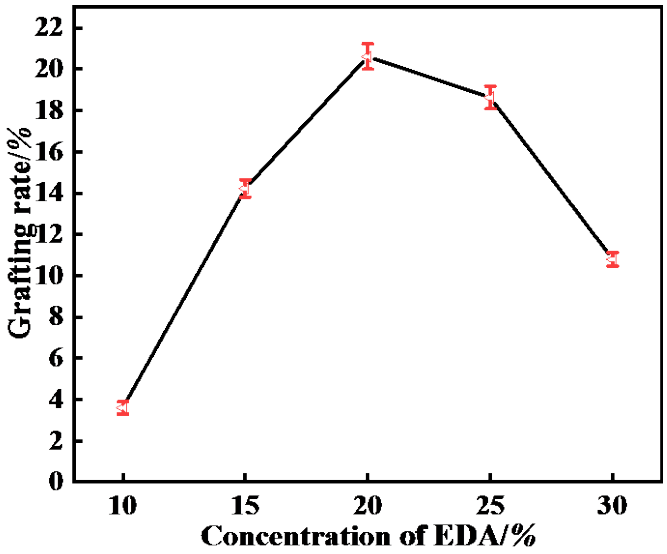

Fig. S3 The grafting rate of PAN/AC nanofibers with different concentrations of EDA.

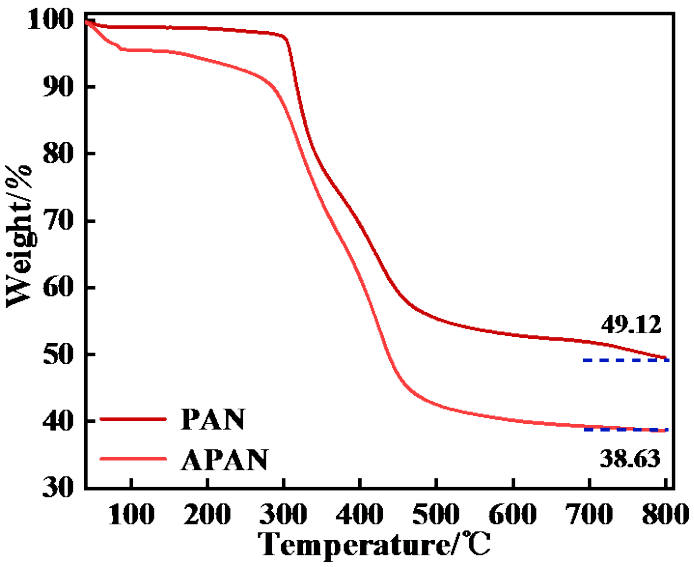

Fig. S4 TGA curves of PAN and APAN nanofibers.

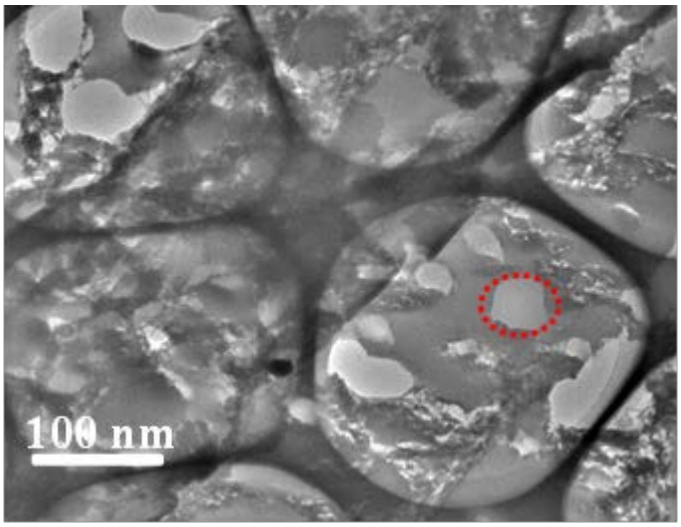

Fig. S5 Cross section TEM of APAN/AC nanofibers.

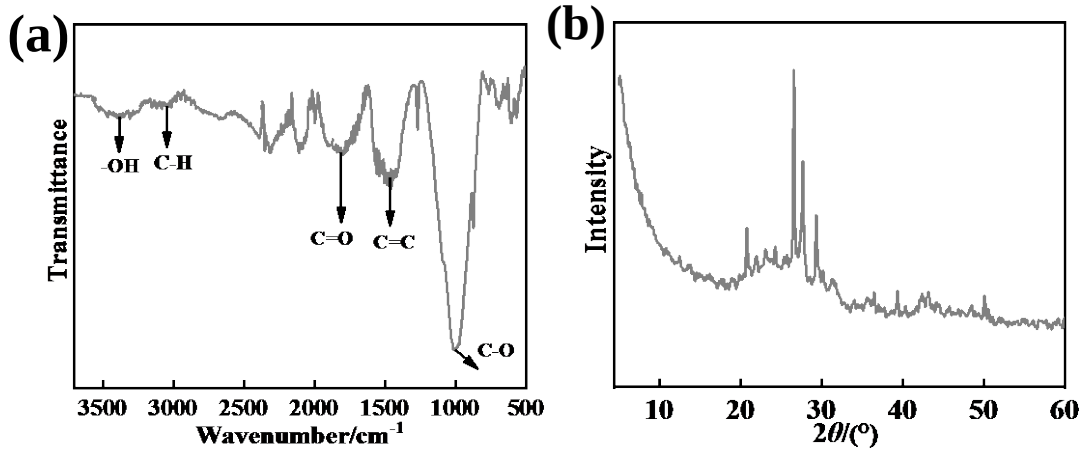

Fig. S6 FTIR and XRD spectrum of the AC.

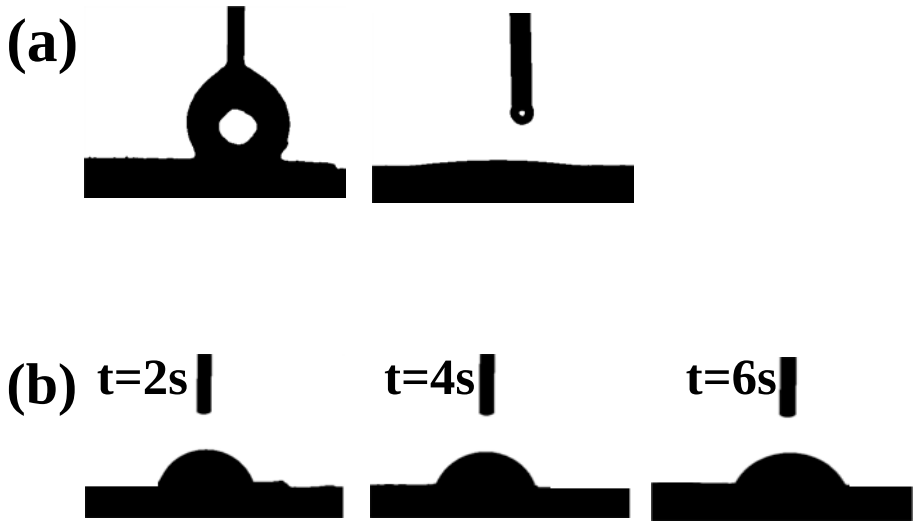

Fig. S7 Change of the water contact angles of (a) AC and (b) PAN nanofibers.

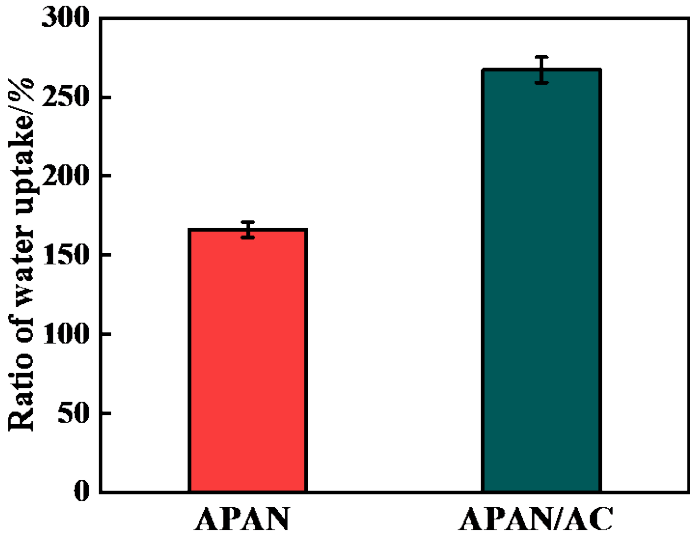

Fig. S8 The water uptake capacity of APAN and APAN/AC nanofibers.

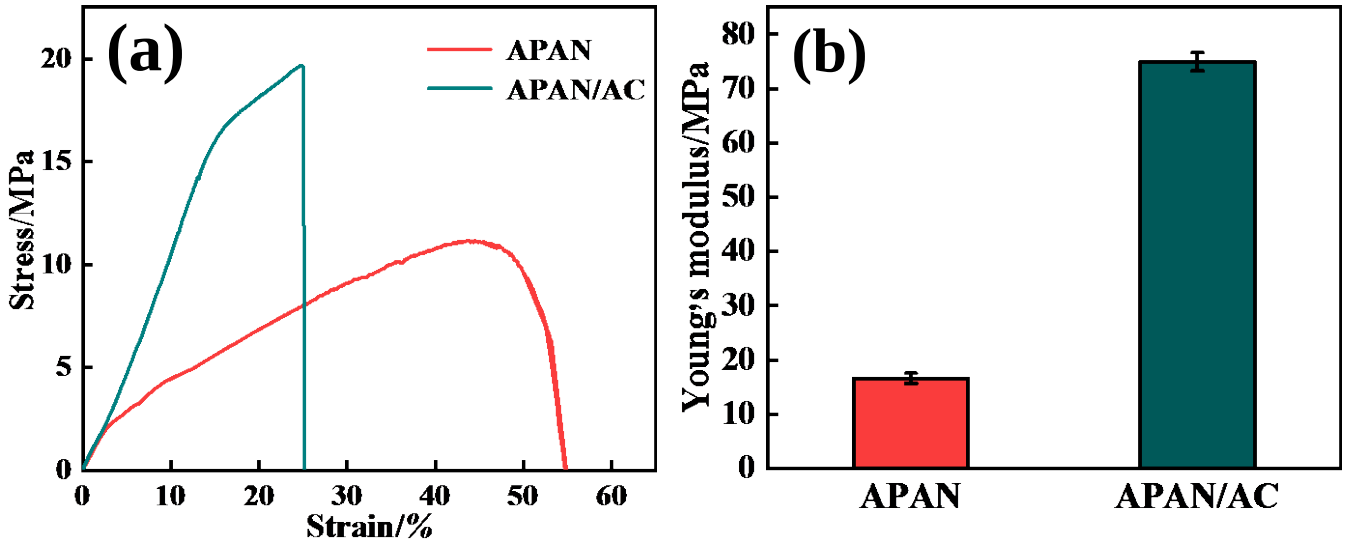

Fig. S9 (a) Tensile stress-strain curves and (b) Young's module of APAN and APAN/AC nanofibers.

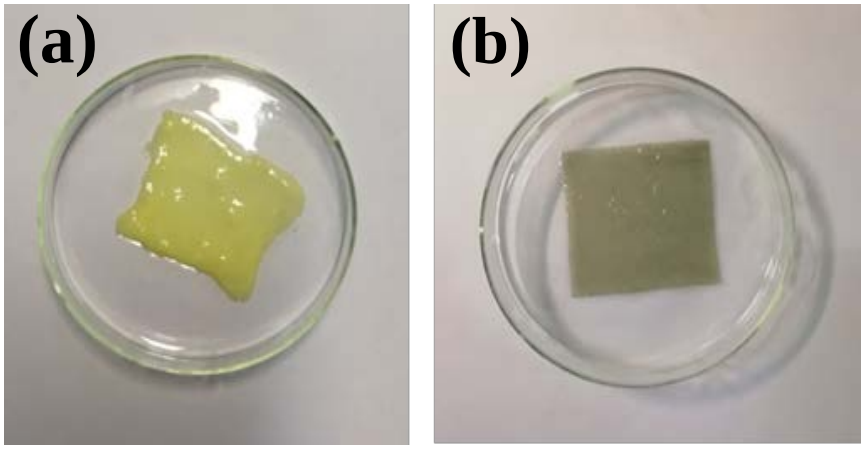

Fig. S10 The digital photos under identical ammoniating condition of (a) APAN and (b) APAN/AC nanofibers.

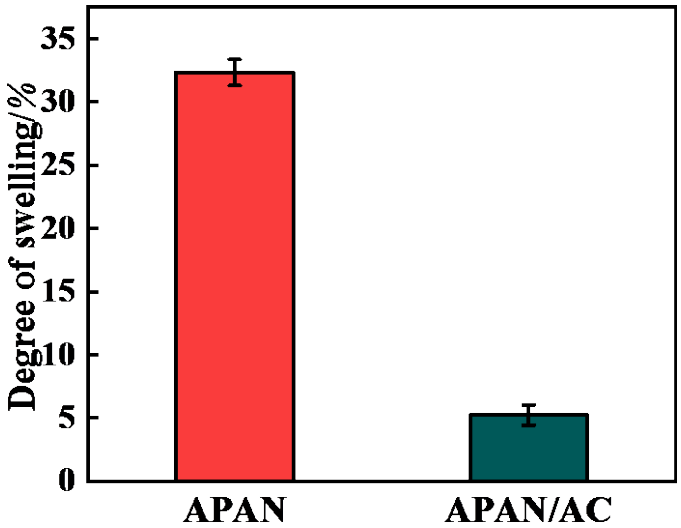

Fig. S11 The degree of swelling of APAN and APAN/AC nanofibers.

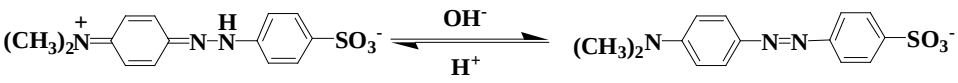

Fig. S12 Chemical structure of MO.

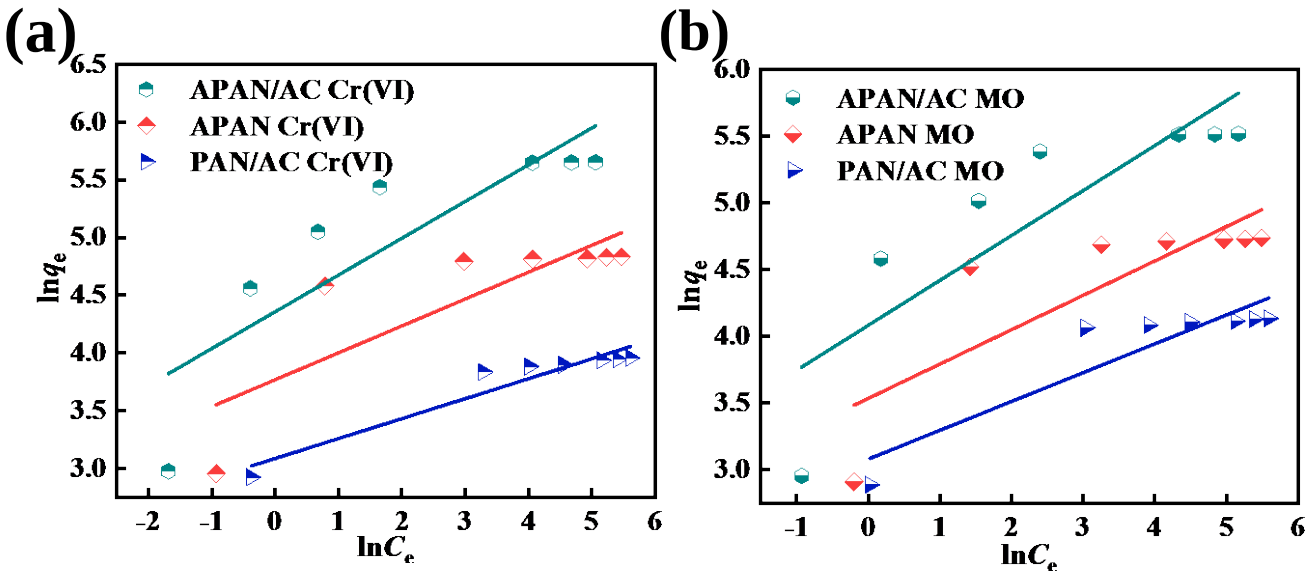

Fig. S13 Freundlich isotherm plots for APAN/AC, APAN and PAN/AC nanofibers of (a) Cr(VI) and (b) MO.

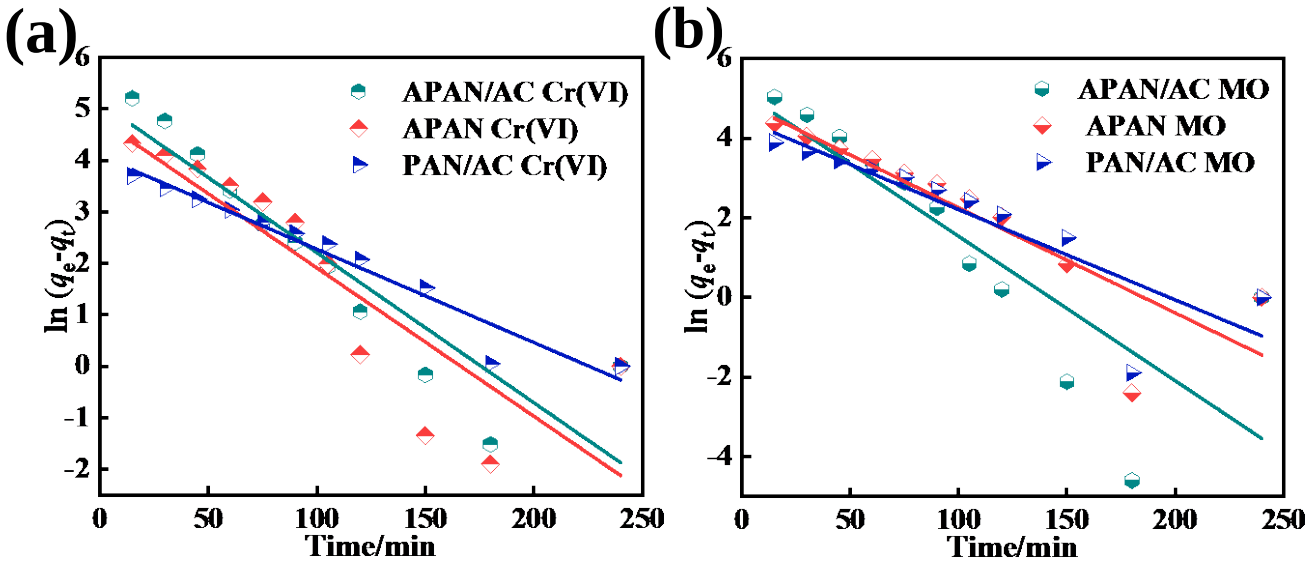

Fig S14. Pseudo-first-order kinetic plots for APAN/AC, APAN and PAN/AC nanofibers of (a) Cr(VI) and (b) MO.

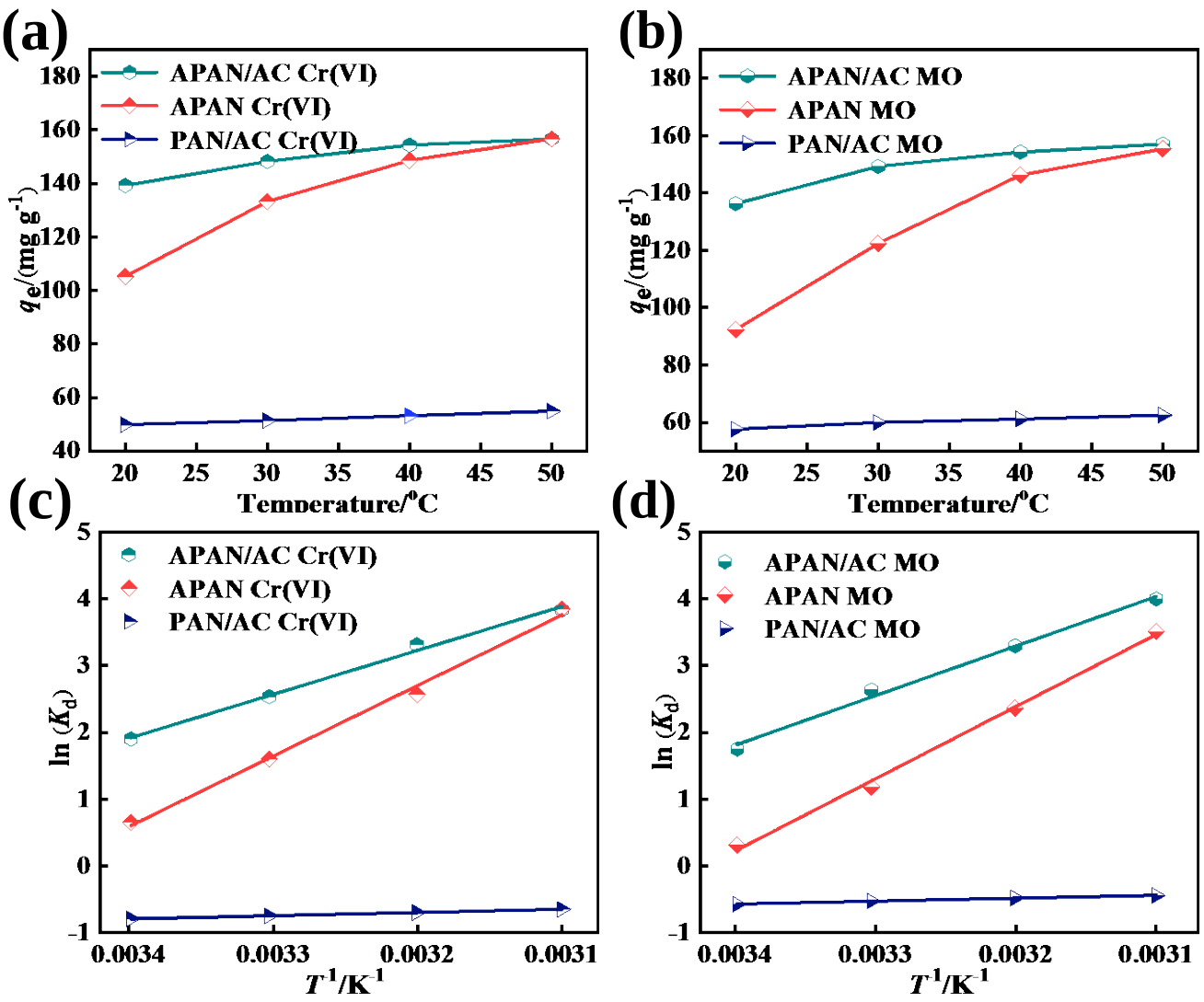

Fig S15 The effect of temperature plots for APAN/AC, APAN and PAN/AC nanofibers of (a) Cr(VI) and (b) MO, and dependence of ln K_d values on 1/T for c) Cr(VI) and d) MO.

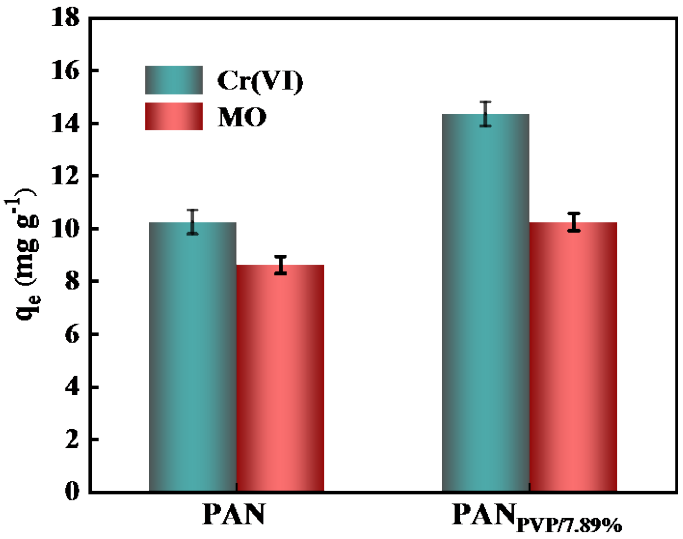

Fig. S16 The adsorption capacity of PAN and $PAN_{PVP/7.89\%}$ nanofibers.

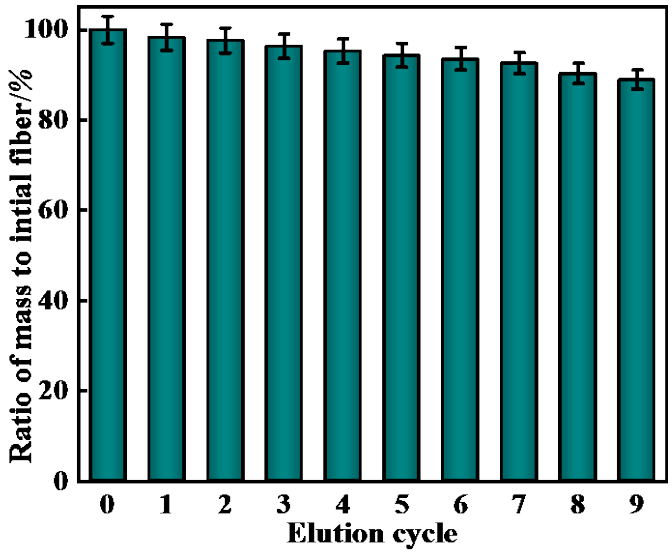

Fig. S17 The mass change of APAN/AC nanofibers after each round of elution.

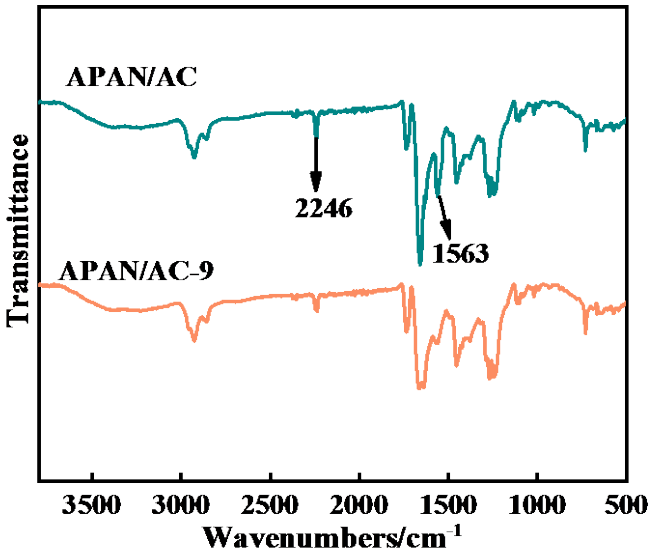

Fig. S18 FTIR spectra of APAN/AC and recycled APAN/AC nanofibers.

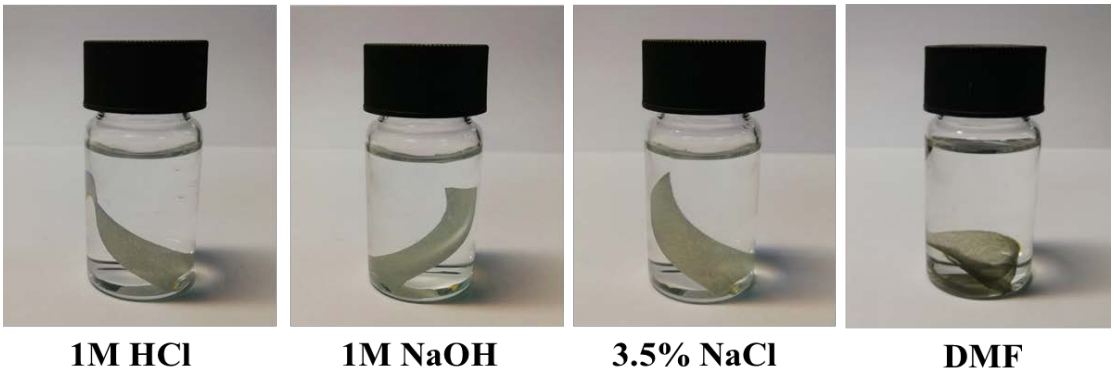

Fig. S19 The effect of stability of APAN/AC nanofibers at acid, base, salt, and polar solvents.

Table S1 The ratio of the initial added AC to PAN nanofibers.

AC/g	PAN/g	PVP/g	AC/PAN weight ratio
0	0.75	0.75	0
0.0375	0.75	0.75	0.05
0.0750	0.75	0.75	0.10
0.1125	0.75	0.75	0.15
0.150	0.75	0.75	0.20
0.1875	0.75	0.75	0.25

Table S2 Comparison of the maximum adsorption capacity for Cr(VI) on different adsorbents.

Adsorbents	q_e /(mg g^{-1})	References
Ficusglomerata	23	[1]
Polyacrylonitrile fiber	32	[2]
Hydrochar-PEI	33	[3]
Apple peels	36	[4]
Water-insoluble cross-linked PEI (CPEI)	40	[5]
MWCNTs-PEI	40	[5]
Rice husk-PEI	43	[6]
Magnetic Nanocarbon	43	[7]
Carbonaceous	54	[8]
nanofibrous composite microfiltration membranes	67	[9]
Paper-PEI	68	[10]
Halloysite nanotubes-PEI	103	[11]
APF	133	[12]
Populus fiber-g-PA	180	[13]
APAN/AC	284	This Work

Table S3 Comparison of the maximum adsorption capacity for MO on different adsorbents.

Adsorbents	q_e /(mg g^{-1})	References
Multiwall carbon nanotubes (MWCNT)	50	[14]
Konjac glucomannan/graphene oxide hydrogel	52	[15]
Protonated cross-linked chitosan	89	[16]
EDTA functionalized Polyacrylonitrile (PAN/EDTA)	99	[17]
Carbon-coated monolith	102	[18]
PAN/PAMAM Blend Nanofiber Mats	120	[19]
Polyimide-derived laser-induced graphene	132	[20]
N-doped mesoporous carbon (N-OMC)	136	[21]
Acid-functionalized carbon coated monolith	147	[22]
Alkali-activated multi-walled carbon nanotubes	149	[14]
N-doped mesoporous carbon	151	[21]
Activated carbon/$NiFe_2O_4$ magnetic composite	183	[23]
PCs-0.5-800	188	[24]
Fe_3O_4-N-doped mesoporous carbon	200	[25]
APAN/AC	248	This Work

Table S4 The thermodynamic parameters of APAN and PAN/AC nanofibers.

Temperature/K		ΔG^0 /(kJ mol^{-1})		ΔH^0 /(kJ mol^{-1})		ΔS^0 /(J mol^{-1} K^{-1})	
		APAN	PAN/AC	APAN	PAN/AC	APAN	PAN/AC
Cr（VI)	293	-1.1	-0.14	81.89	2.18	303.74	7.92
	303	-4.14	-0.22				
	313	-7.18	-0.32				
	323	-10.21	-0.38				
MO	293	-0.21	-0.086	89.90	2.43	307.53	8.59
	303	-3.28	-0.17				
	303	-6.36	-0.26				
	323	-9.43	-0.34				

Supporting calculation formula

The mass ratio of PAN: PVP: AC was 1:1:0.5 in the PAN/PVP/AC nanofibers. Then, the mass of PVP (W_0, g) inside PAN/PVP/AC nanofibers and the mass loss of PVP (W_1, g) during water treatment were calculated. The proportion of remained PVP (R_{PVP}) was calculated as follows:

$$R_{PVP}(\%) = \frac{W_0 - W_1}{W_0} \times 100 \quad \text{(S1)}$$

$$Grafting\ rate\,(\%) = (\frac{W_2 - W_3}{W_2}) \times 100 \quad \text{(S2)}$$

Where, W_2 (g) and W_3 (g) represent the weights before and after PAN/AC grafting, respectively.

Supporting References

1. Rao R A K, Rehman F. Adsorption studies on fruits of Gular (Ficus glomerata): Removal of Cr(VI) from synthetic wastewater. Journal of Hazardous Materials, 2010, 181(1): 405-412

2. Bouchoum H, Benmoussa D, Jada A, Tahiri M, Cherkaoui O. Synthesis of amidoximated polyacrylonitrile fibers and its use as adsorbent for Cr (VI) ions removal from aqueous solutions. Environmental Progress & Sustainable Energy, 2019, 38: 13196

3. Shi Y, Zhang T, Ren H, Kruse A, Cui R. Polyethylene imine modified hydrochar adsorption for chromium (VI) and nickel (II) removal from aqueous solution. Bioresource Technology, 2018, 247: 370-379

4. Enniya I, Rghioui L, Jourani A. Adsorption of hexavalent chromium in aqueous solution on activated carbon prepared from apple peels. Sustainable Chemistry and Pharmacy, 2018, 7: 9-16

5. Sambaza S S, Masheane M L, Malinga S P, Nxumalo E N, Mhlanga S D. Polyethyleneimine-carbon nanotube polymeric nanocomposite adsorbents for the removal of Cr^{6+} from water. Physics and Chemistry of the Earth, Parts A/B/C, 2017, 100: 236-246

6. Jiang X, An Q D, Xiao Z Y, Zhai S R, Shi Z. Mussel-inspired surface modification of untreated wasted husks with stable polydopamine/polyethylenimine for efficient continuous Cr(VI) removal. Materials Research Bulletin, 2018, 102: 218-225

7. Huang J, Cao Y, Shao Q, Peng X, Guo Z. Magnetic nanocarbon adsorbents with enhanced hexavalent chromium removal: Morphology dependence of fibrillar vs particulate structures. Industrial & Engineering Chemistry Research, 2017, 56(38): 10689-10701

8. Jain M, Garg V K, Kadirvelu K. Adsorption of hexavalent chromium from aqueous medium onto carbonaceous adsorbents prepared from waste biomass. Journal of Environmental Management, 2010, 91(4): 949-957

9. Liu X, Jiang B, Yin X, Ma H, Hsiao B S. Highly permeable nanofibrous composite microfiltration membranes for removal of nanoparticles and heavy metal ions. Separation and Purification Technology, 2020, 233: 115976

10. Setyono D, Valiyaveettil S. Functionalized paper-A readily accessible adsorbent for removal of dissolved heavy metal salts and nanoparticles

from water. Journal of Hazardous Materials, 2016, 302: 120-128

11. Tian X, Wang W, Wang Y, Komarneni S, Yang C. Polyethylenimine functionalized halloysite nanotubes for efficient removal and fixation of Cr (VI). Microporous and Mesoporous Materials, 2015, 207: 46-52

12. Tangtubtim S, Saikrasun S. Adsorption behavior of polyethyleneimine-carbamate linked pineapple leaf fiber for Cr(VI) removal. Applied Surface Science, 2019, 467-468: 596-607

13. Li M, Gong Y, Lyu A, Liu Y, Zhang H. The applications of populus fiber in removal of Cr(VI) from aqueous solution. Applied Surface Science, 2016, 383: 133-141

14. Ma J, Yu F, Zhou L, Jin L, Yang M, Luan J, Tang Y, Fan H, Yuan Z, Chen J. Enhanced adsorptive removal of methyl orange and methylene blue from aqueous solution by alkali-activated multiwalled carbon nanotubes. ACS Appl Mater Interfaces, 2012, 4(11): 5749-5760

15. Gan L, Shang S, Hu E, Yuen C, Jiang S X. Konjac glucomannan/graphene oxide hydrogel with enhanced dyes adsorption capability for methyl blue and methyl orange. Applied Surface Science, 2015, 357: 866-872

16. Huang R, Liu Q, Huo J, Yang B. Adsorption of methyl orange onto protonated cross-linked chitosan. Arabian Journal of Chemistry, 2017, 10(1): 24-32

17. Chaúque E F C, Dlamini L N, Adelodun A A, Greyling C J, Ngila J C. Electrospun polyacrylonitrile nanofibers functionalized with EDTA for adsorption of ionic dyes. Physics and Chemistry of the Earth, Parts A/B/C, 2017, 100: 201-211

18. Hosseini S, Khan M A, Malekbala M R, Cheah W, Choong T S Y. Carbon coated monolith, a mesoporous material for the removal of methyl orange from aqueous phase: Adsorption and desorption studies. Chemical Engineering Journal, 2011, 171(3): 1124-1131

19. Hou C, Yang H, Xu Z L, Wei Y. Preparation of PAN/PAMAM blend nanofiber mats as efficient adsorbent for dye removal. Fibers and Polymers, 2015, 16(9): 1917-1924

20. Xiao J, Lv W, Xie Z, Song Y, Zheng Q. l-cysteine-reduced graphene oxide/poly(vinyl alcohol) ultralight aerogel as a broad-spectrum adsorbent for anionic and cationic dyes. Journal of Materials Science, 2017, 52(10): 5807-5821

21. Sánchez Sánchez Á, Suárez García F, Martínez Alonso A, Tascón J M D. Synthesis, characterization and dye removal capacities of N-doped mesoporous carbons. Journal of Colloid and Interface Science, 2015, 450: 91-100

22. Cheah W, Hosseini S, Khan M A, Chuah T G, Choong T S Y. Acid modified carbon coated monolith for methyl orange adsorption. Chemical Engineering Journal, 2013, 215-216: 747-754

23. Jiang T, Liang Y D, He Y J, Wang Q. Activated carbon/$NiFe_2O_4$ magnetic composite: A magnetic adsorbent for the adsorption of methyl orange. Journal of Environmental Chemical Engineering, 2015, 3(3): 1740-1751

24. Sun B, Yuan Y, Li H, Li X, Zhang C, Guo F, Liu X, Wang K, Zhao X S. Waste-cellulose-derived porous carbon adsorbents for methyl orange removal. Chemical Engineering Journal, 2019, 371: 55-63

25. Liang T, Wang F, Liang L, Liu M, Sun J. Magnetically separable nitrogen-doped mesoporous carbon with high adsorption capacity. Journal of Materials Science, 2016, 51(8): 3868-3879